

DETC2012-70943

BIFURCATIONS IN TWINKLING OSCILLATORS

Smruti R. Panigrahi*

Dynamics and Vibrations
Research Laboratory
Department of Mechanical Engineering
Michigan State University
E. Lansing, Michigan, 48824
Email: smruti@msu.edu
Phone: 517-515-1620

Brian F. Feeny

Department of Mechanical Engineering
Michigan State University
E. Lansing, Michigan, 48824
Email: feeny@egr.msu.edu
Phone: 517-353-9451
Fax: 517-353-1750

Alejandro R. Diaz

Department of Mechanical Engineering
Michigan State University
E. Lansing, Michigan, 48824
Email: diaz@egr.msu.edu
Phone: 517-353-9861
Fax: 517-353-1750

ABSTRACT

We present the underlying dynamics of snap-through structures that exhibit twinkling. Twinkling occurs when the nonlinear structure is loaded slowly and the masses snap-through, converting the low frequency input to high frequency oscillations. We have studied a nonlinear spring-mass chain loaded by a quasistatic pull. The spring forces are assumed to be cubic with intervals of negative stiffness. Depending on the parameters, the system has equilibria at multiple energy levels. The normal form and the bifurcation behaviors for the single and two degree of freedom systems are studied in detail. A new type of bifurcation, which we refer to as a star bifurcation, has been observed for the symmetric two degree of freedom system, which is of codimension four for the undamped case, and codimension three or two for the damped case, depending on the form of the damping.

Keywords: Energy Harvesting, Negative Stiffness, Bifurcation, Codimension, Twinkling Oscillator, Star Bifurcation

1 Introduction

This work is motivated by the idea of using snap-through structures to induce high frequency oscillations from low frequency ambient vibrations to harvest energy. Several authors have studied the dynamics of various snap-through negative stiffness and bistable systems [1–5]. Nonlinear massless static electric-springs [6], and magneto static-springs [7] have been studied numerically. Vibration based energy harvesting from linear systems [8, 9] has been optimized experimentally [10–12] by tun-

ing the forcing frequency to the natural frequency of the oscillator. Piezoelectric materials have been used for successful experimental energy harvesting from vibrating sources [8, 9, 13–15] and fluctuating pressure load [16, 17]. Nonlinear spring-mass systems have the potential to harvest energy from a variety of sources such as ambient vibrations, earthquake, low frequency seismic phenomenon and tsunami. In this work, we look at the behavior of snap-through spring-mass oscillations.

Nonlinearity has been studied by several authors for energy management. For example, essential nonlinearity has been used as a nonlinear energy sink (NES) for energy harvesting [18–20], nonlinear energy pumping [21–23], and nonlinear targeted energy transfer (TET) [24–28]. Novel ways of experimental energy harvesting have been achieved from low frequency ambient excitations [14, 15, 29, 30] and nonlinear oscillations of magnetic levitations [31]. Wireless Energy Transfer (WET) has recently become the subject of renewed research in the scientific community since past few years [32–37], after the concept was first introduced almost one century ago by Nikola Tesla [38]. Both of these concepts of TET in NES system and WET can be used to harvest energy using piezoelectric materials, and transfer energy across devices and mediums respectively. The snap-through structures, possibly in the scale of a MEMS device, can be installed in the WET device that can be triggered by magnetic excitation from the WET source, to induce a high frequency oscillation in the snap through system, thereby allowing the power harvesting in the device while the energy transfer is performed by the WET source.

*Address all correspondence to this author.

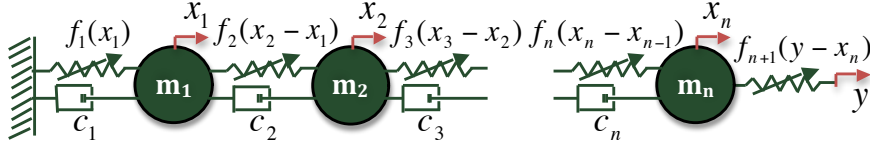


FIGURE 1. n -degree-of-freedom spring-mass chain connected by n masses, $(n + 1)$ nonlinear springs, and n dash-pots. As shown in this figure the left spring is fixed to a base and the right most spring is pulled quasistatically to a distance y_0 .

In this article we explore the dynamics of a nonlinear mass chain with cubic springs, that have three distinct roots in the characteristic. The chain is connected to a fixed base at one end and to a pulled point at the other end, as shown in Figure 1. The end spring is then pulled quasistatically to a certain distance to observe the “twinkling phenomenon” in the chain. As this pull parameter is changed we see high frequency oscillations about different equilibrium states. While the system goes through all the bifurcations, it exhibits complicated behaviors in the phase space. As the system exhibits twinkling phenomenon and comes to an equilibrium state due to small applied damping, it contains a total energy that was not present in the system before the applied quasistatic pull. This residual energy will be of importance to energy harvesting and WET. Final equilibria of this type of twinkler have differing energy states. Predicting the final energy of the system requires analysis of transients, which are influenced by the structure of both stable and unstable equilibria. In this article we first study the local bifurcation behavior. We will be presenting the stability analysis and the related degree of degeneracy using the concept of codimension, and show how the codimension of the system changes with damping.

In section 2, we construct the nonlinear ODE from the equation of motion (EOM), and discuss the conditions for the stability. In section 3, we will perform a coordinate transformation and obtain a normal form for the initial bifurcation in a single and a two DOF system. Finally in section 4, we will present our final remarks by ending the article with the targeted application areas and future research works in the area.

2 Snap-Through Structures: Twinkler

The equations of motion (EOM) of an n -degree-of-freedom (n -DOF) snap-through system as shown in the Figure 1, written using the Newton’s second law of motion, as

$$\begin{aligned} m_1 \ddot{x}_1 + c_1 \dot{x}_1 - c_2 (\dot{x}_2 - \dot{x}_1) &= f_2(x_2 - x_1) - f_1(x_1) \\ m_i \ddot{x}_i + c_i (\dot{x}_i - \dot{x}_{i-1}) - c_{i+1} (\dot{x}_{i+1} - \dot{x}_i) &= \\ f_{i+1}(x_{i+1} - x_i) - f_i(x_i - x_{i-1}); \forall i = 2, 3, \dots, n-1 \\ m_n \ddot{x}_n + c_n (\dot{x}_n - \dot{x}_{n-1}) &= f_{n+1}(y - x_n) - f_n(x_n - x_{n-1}) \end{aligned} \quad (1)$$

where m_i is the i^{th} mass, c_i is the damping of the i^{th} spring and y is the quasistatic pull as shown in the Figure 2, applied to the

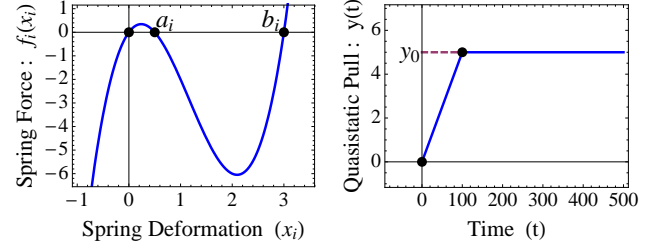


FIGURE 2. The characteristic spring force $f_i(x_i)$ of the nonlinear spring as a function of the spring deformation x_i , and the quasistatic pull as a function of time.

end spring. Dividing by the masses, the undamped system can be written in the form

$$\ddot{\mathbf{x}} = \mathbf{f}(\mathbf{x}) \quad (2)$$

A cubic spring with the spring force $f_i(x_i)$ is considered to be of the form

$$f_i(x_i) = \gamma_i x_i (x_i - a_i) (x_i - b_i); \quad \forall i = 1, 2, \dots, n+1 \quad (3)$$

Referring to the Figure 1, as the end spring is pulled quasistatically until $y = y_0$, we examine the equilibria. At equilibrium both the accelerations and the velocities of all the masses go to zero, hence we get the following array of equations for the n -DOF structure:

$$\begin{aligned} f_2(x_2 - x_1) &= f_1(x_1) \\ f_{i+1}(x_{i+1} - x_i) &= f_i(x_i - x_{i-1}); \quad \forall i = 2, 3, \dots, n-1 \\ f_{n+1}(y_0 - x_n) &= f_n(x_n - x_{n-1}) \end{aligned} \quad (4)$$

As we solve the equation (4) we find the bifurcation behavior with respect to y_0 . The stabilities of the equilibria of the second order ordinary differential equation (2) can be found by computing the eigenvalues of the Jacobian of \mathbf{f} . For a second order undamped equation the stabilities are determined as shown in the following equations:

$$\ddot{\mathbf{x}} = [\mathbf{Df}] \mathbf{x} = -\tilde{\mathbf{K}} \mathbf{x}, \quad \text{where } \tilde{\mathbf{K}} = -[\mathbf{Df}] \Rightarrow \ddot{\mathbf{x}} + \tilde{\mathbf{K}} \mathbf{x} = 0 \quad (5)$$

Assuming a response of the form $\mathbf{x} = e^{\pm i\omega t} \phi$, the eigenvalue problem becomes

$$[\tilde{\mathbf{K}} - \omega^2 \mathbf{I}] \phi = 0 \Rightarrow \lambda = \omega^2 \quad (6)$$

where ω are the eigenfrequencies, λ are the eigenvalues and ϕ are the eigenvectors. If $\lambda < 0$ there is an exponential solution that blows up as time t increases, a stable oscillatory solution exists for $\lambda > 0$, and neutrally stable solutions for $\lambda = 0$:

$$\begin{aligned} \mathbf{x} &= \mathbf{A}_1 e^{\sqrt{-\lambda}t} + \mathbf{A}_2 e^{-\sqrt{-\lambda}t} & \forall \lambda < 0 \\ \mathbf{x} &= \mathbf{A}_1 e^{i\sqrt{\lambda}t} + \mathbf{A}_2 e^{-i\sqrt{\lambda}t} & \forall \lambda > 0 \end{aligned} \quad (7)$$

Thus, in the second order undamped form, a bifurcation is indicated as a single eigenvalue passes through zero, corresponding to a transition of a second-order oscillation to a second-order saddle (in a two-dimensional phase space). Equivalently, it corresponds to a stiffness going from positive to negative.

Now we need to formulate the problem for a n-DOF system in order to be able to solve it numerically in the first order form. The second order nonlinear ODE for a n-DOF system in the vector form is:

$$\mathbf{M}\ddot{\mathbf{x}} + \mathbf{C}\dot{\mathbf{x}} + \mathbf{K}\mathbf{x} = \mathbf{f}_{nl} \quad (8)$$

where \mathbf{x} is an $n \times 1$ array of mass displacements, \mathbf{M} , \mathbf{C} , and \mathbf{K} , are the $n \times n$ mass, damping, and stiffness matrices, \mathbf{f}_{nl} is the nonlinear part of the spring force. Specifically,

$$\mathbf{K} = \begin{pmatrix} k_1 + k_2 & -k_2 & 0 & \cdots & 0 & 0 \\ -k_2 & k_2 + k_3 & -k_3 & \cdots & 0 & 0 \\ \vdots & \vdots & \vdots & \ddots & \vdots & \vdots \\ 0 & 0 & 0 & \cdots & k_{n-1} + k_n & -k_n \\ 0 & 0 & 0 & \cdots & -k_n & k_n \end{pmatrix} \quad (9)$$

where $k_i = \gamma_i a_i b_i$, $\forall i = 1, 2, \dots, n+1$

$$\mathbf{f}_{nl} = \begin{pmatrix} \hat{f}_2(x_2 - x_1) - \hat{f}_1(x_1) \\ \vdots \\ \hat{f}_{i+1}(x_{i+1} - x_i) - \hat{f}_i(x_i - x_{i-1}) \\ \vdots \\ \hat{f}_{n+1}(y - x_n) - \hat{f}_n(x_n - x_{n-1}) + \alpha_{n+1}(y - x_n) \end{pmatrix} \quad (10)$$

where $\hat{f}_i(x_i) = \beta_i x_i^2 + \gamma_i x_i^3$, $\alpha_i = \gamma_i a_i b_i$ and $\beta_i = -\gamma_i(a_i + b_i)$, $\forall i = 1, 2, \dots, n+1$. For our analysis, the second order ordinary differential equations for the n-DOF system are converted into first order differential equations by defining a $2n \times 1$ state vector

$$\mathbf{z} = \begin{Bmatrix} \mathbf{z}_1 \\ \mathbf{z}_2 \end{Bmatrix} = \begin{Bmatrix} \dot{\mathbf{x}} \\ \mathbf{x} \end{Bmatrix} \quad (11)$$

where $\mathbf{z}_1 = \dot{\mathbf{x}}$, $\mathbf{z}_2 = \mathbf{x}$, and $\dot{\mathbf{z}}_2 = \mathbf{z}_1$, yielding unforced equations of motion of the form

$$\mathbf{A}\dot{\mathbf{z}} = \mathbf{J}\mathbf{z} + \tilde{\mathbf{f}} \quad (12)$$

$$\text{where } \mathbf{A} = \begin{bmatrix} \mathbf{M} & \mathbf{0} \\ \mathbf{0} & \mathbf{I} \end{bmatrix}, \quad \mathbf{J} = \begin{bmatrix} -\mathbf{C} & -\mathbf{K} \\ \mathbf{I} & \mathbf{0} \end{bmatrix}, \quad \tilde{\mathbf{f}} = \begin{Bmatrix} \mathbf{f}_{nl} \\ \mathbf{0} \end{Bmatrix} \quad (13)$$

\mathbf{A} and \mathbf{J} are $2n \times 2n$ matrices and $\tilde{\mathbf{f}}$ is $2n \times 1$ vector. We use the above equation (12) for the twinkler to obtain the numerical solution in a SDOF and 2DOF system and study the bifurcation behaviors with respect to the parameter y_0 .

3 Bifurcation Behaviors of the Twinkler

The cubic nonlinearity in the twinkler gives rise to multiple equilibria for the parameter region where the twinkler passes through the negative stiffness region. We used a coordinate transformation to simplify the form for the analysis of the bifurcation events. This provides something like a normal form for the system of second order equations. For n-DOF twinkler we obtain the equilibrium solutions from the equation (4). For symmetric case, all the spring forces are identical, hence $\gamma_i = \gamma$, $a_i = a$ and $b_i = b$. For all computations, we have used $\gamma = 2$, $a = 0.5$, and $b = 3.0$. The values of a and b are chosen to represent a stiffness function of a spring that is preloaded to be somewhat near snap through.

3.1 Bifurcations in SDOF Twinkler

For the SDOF system, equilibrium is attained when $f_1(x) = f_2(y_0 - x)$. Therefore, the equilibrium equation is:

$$\begin{aligned} \gamma_1 x(x - a_1)(x - b_1) \\ = \gamma_2(y_0 - x)((y_0 - x) - a_2)((y_0 - x) - b_2) \end{aligned} \quad (14)$$

In this SDOF system, we observe two pitchfork bifurcations at B_1 and B_2 as shown in the Figure 3, when the symmetric system snaps through, providing a parameter interval in which two stable and one unstable equilibria exist. Breaking the symmetry typically breaks the pitchforks into saddle-node bifurcations, preserving the interval of two coexisting stable equilibria. For the lightly damped symmetric system, one zero eigenvalue at the bifurcation point can be referred to as a codimension [39,40] one bifurcation, which however is a codimension two bifurcation in the undamped system as both the eigenvalues go to zero. The global symmetry breaking bifurcation behavior reveals the presence of multiple energy levels, in the negative stiffness region.

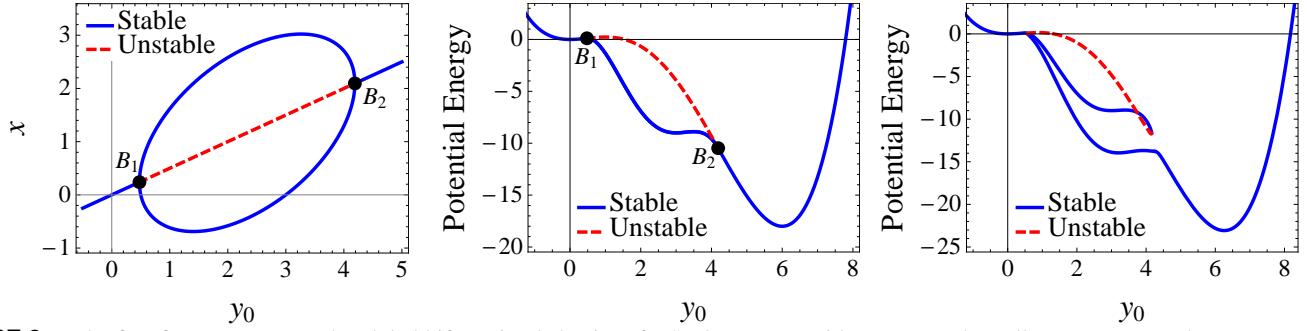


FIGURE 3. The first figure represents the global bifurcation behavior of a SDOF system with respect to the pull parameter y_0 . The next two figures represent the total spring potential energy of the system at the final equilibrium state. The middle figure shows two overlapping energy levels in the negative stiffness region that are revealed with an applied perturbation in the right figure, where $a_2 = a + \varepsilon$ and $b_2 = b + \varepsilon$, for $\varepsilon = 0.1$.

3.2 Bifurcations in 2DOF Twinkler

We will study the dynamics of the 2DOF system to understand the system behavior as the oscillations settle down to an equilibrium configuration. At equilibrium the velocities and accelerations of both the masses dies down to zero, resulting in $f_1(x_1) = f_2(x_2 - x_1)$ and $f_2(x_2 - x_1) = f_3(y_0 - x_2)$. Therefore the equilibrium equation is written as

$$\begin{aligned} \gamma_1 x_1 (x_1 - a_1) (x_1 - b_1) \\ &= \gamma_2 (x_2 - x_1) ((x_2 - x_1) - a_2) ((x_2 - x_1) - b_2) \\ \gamma_2 (x_2 - x_1) ((x_2 - x_1) - a_2) ((x_2 - x_1) - b_2) \\ &= \gamma_3 (y_0 - x_2) ((y_0 - x_2) - a_3) ((y_0 - x_2) - b_3) \end{aligned} \quad (15)$$

For the symmetric case, $\gamma_i = \gamma$, $a_i = a$, and $b_i = b$, for $i = 1, 2, 3$. For all computations we have used $\gamma = 2$. The numerical solution of the equilibrium for this 2DOF spring mass system results in the bifurcation curves as figure 4. We transform the coordinates to simplify the EOM. The change of coordinates is done by first moving the origin to the bifurcation point, and then rotating the lines $x_1 = \frac{y_0}{3}$ and $x_2 = \frac{2y_0}{3}$ to coincide with the horizontal axis, using $y_0 = p + y_b$, $x_1 = u_1 + \frac{p+y_b}{3}$, and $x_2 = u_2 + \frac{2(p+y_b)}{3}$.

Now (p, u_1, u_2) are the new coordinates of the transformed system and the expression for y_b is obtained later in this section. Plugging the above transformations into equation (1), and letting $c_1 = c_2 = c$, for the symmetric system, we get the transformed damped EOM,

$$\begin{aligned} \ddot{u}_1 + 2c\dot{u}_1 - c\dot{u}_2 &= 2(u_2 - 2u_1)(A - u_2 y_1 + p u_2) \\ \ddot{u}_2 - c\dot{u}_1 + c\dot{u}_2 &= 2(u_1 - 2u_2)(A + u_1 y_1 - p u_1) \end{aligned} \quad (16)$$

where $A = (u_1^2 - u_1 u_2 + u_2^2 - \frac{2p y_1}{3} + \frac{p^2}{3})$, and $y_1 = (a + b - y_b)$. At equilibrium $\ddot{u}_1 = \ddot{u}_2 = 0$, $\dot{u}_1 = \dot{u}_2 = 0$. Therefore the trans-

formed equilibrium condition for the 2DOF twinkler,

$$\begin{aligned} g_1(u_1, u_2, p) &= 2(u_2 - 2u_1)(A - u_2 y_1 + p u_2) = 0 \\ g_2(u_1, u_2, p) &= 2(u_1 - 2u_2)(A + u_1 y_1 - p u_1) = 0 \end{aligned} \quad (17)$$

The solutions to the above equilibrium equations are

$$\begin{aligned} (u_1, u_2) &= \{(0, 0), (-2p_1, -p_1), (-2p_2, -p_2), \\ &\quad (p_1, -p_1), (p_2, -p_2), (p_2, 2p_2), (p_1, 2p_1)\} \end{aligned} \quad (18)$$

where $p_1 = \frac{1}{6}(p - y_1 + \sqrt{y_1^2 + 6y_1 p - 3p^2})$ and $p_2 = \frac{1}{6}(p - y_1 - \sqrt{y_1^2 + 6y_1 p - 3p^2})$, which have elliptical solution curves as shown in Figure 5. The stabilities of the equilibria curves are determined from the eigenvalues as discussed in equations (5) - (7). Combining the EOMs in equation (17), we get

$$\begin{aligned} (u_1 + u_2)((p - y_1)(3(u_1 - u_2) + 2p) - p^2 - 3u_1 u_2 \\ + 3u_1^2 + 3u_2^2 - (y_b^2 - 2(a + b)y_b + 3ab)) = 0 \end{aligned} \quad (19)$$

We note that the condition $(u_1 + u_2) = 0$, on the equilibria curves $(u_1, u_2) = \{(0, 0), (p_1, -p_1), (p_2, -p_2)\}$ satisfy the equation (19), whereas the other four solution branches do not satisfy this condition for all values of p . Hence for the equation (19) to be satisfied by the other four solution branches, specifically at $p = 0$ i.e. for $(u_1, u_2) = \{(0, 0), (\frac{2y_1}{3}, \frac{y_1}{3}), (\frac{y_1}{3}, -\frac{2y_1}{3}), (0, 0)\}$, we must apply the following constraint,

$$\begin{aligned} y_b^2 - 2(a + b)y_b + 3ab &= 0 \\ \therefore y_b &= a + b - \sqrt{a^2 - ab + b^2} \end{aligned} \quad (20)$$

Since we are moving our coordinate system to the bifurcation point B_1 , here we consider the smaller value of y_b . The other

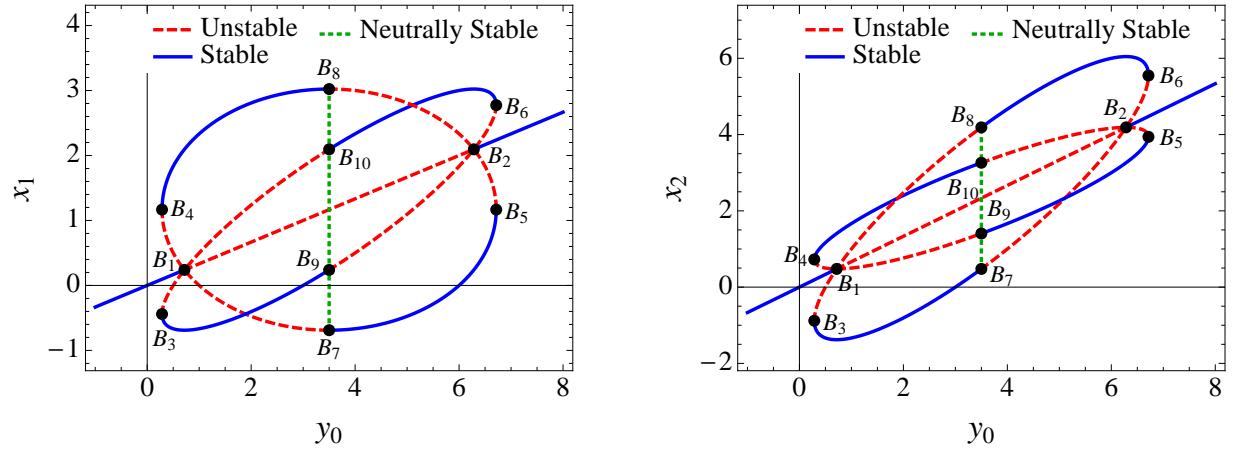


FIGURE 4. The bifurcation diagram for the equilibrium solutions of the lightly damped symmetric 2DOF system with respect to the pull parameter y_0 , where B_1, B_2, \dots, B_{10} are the bifurcation points. The dashed red lines represent unstable solutions, and the solid blue lines represent the stable equilibrium solutions (neutrally stable for the undamped system). The vertical dotted green lines show infinitely many solutions at $y_0 = a + b$, where at the bifurcation points $B_7 - B_{10}$, two of the four eigenvalues are complex conjugates with zero real parts and the other two are zeros for undamped system, whereas with light damping there is one zero, one purely real negative, and the other two are complex conjugate eigenvalues with negative real parts. The bifurcation points $B_3 - B_6$, are saddle-nodes with two zero and two complex conjugate eigenvalues with zero real parts for undamped system, and with light damping there are two complex conjugate eigenvalues with negative real parts, one zero, and one purely real negative eigenvalues.

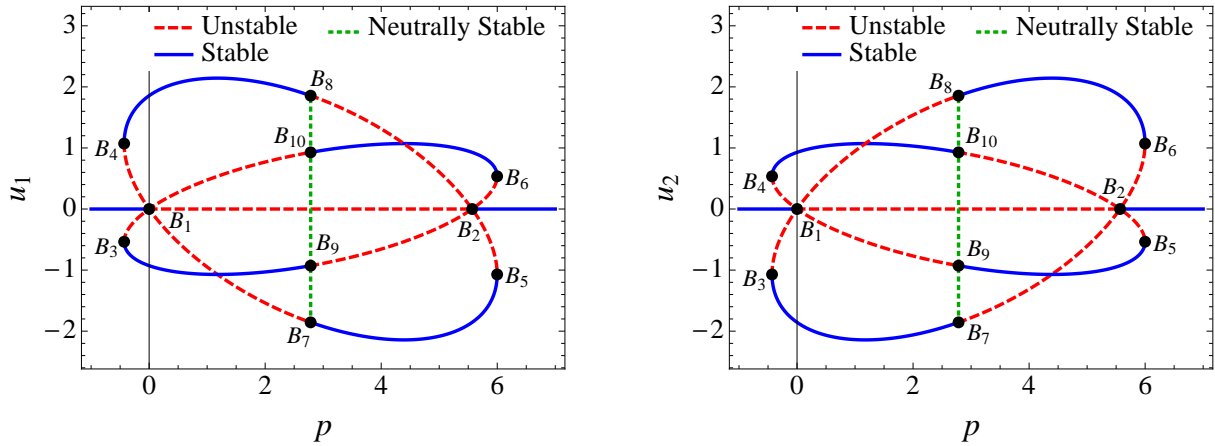


FIGURE 5. The bifurcation diagram for the equilibrium solutions (u_1, u_2) in terms of the pull parameter p are qualitatively similar to the Figure 4, hence the stabilities of the solution curves and the degree of degeneracy of the bifurcation points are inferred.

solution for y_b corresponds to the bifurcation point B_2 . Since both B_1 and B_2 are qualitatively similar we only consider to study the behavior at B_1 .

As p increases, the baseline solution (the horizontal line in Figure 5, and the diagonal straight line in Figure 4) destabilizes in a bifurcation that features a collision of four branches of equilibrium on either side of the bifurcation point. Three branches are visible on either side of the bifurcation point in each figure because the vertical axes of these figures are a projection of a higher dimensional phase space, and some curves overlap in each projection. In both plots in Figure 5, the narrow elliptical curve of equilibria is actually two overlapping elliptical curves.

For convenience, we refer to this bifurcation as a "star bifurcation", as six curves (really eight) emanate from the bifurcation point, in which a neutrally stable (becomes stable when applied a light damping) curve collides simultaneously with three unstable curves to produce four unstable curves. We will study the eigenvalues and the degree of degeneracy of the star bifurcation in the normal form discussed later in this section. Also, as y_0 continues to increase, at $p = y_1 = 2.7838\dots$, the equilibria on the elliptical curves undergo an exchange of stability without intersection. This is also a degenerate type of bifurcation, which we analyze in detail in the follow-up work.

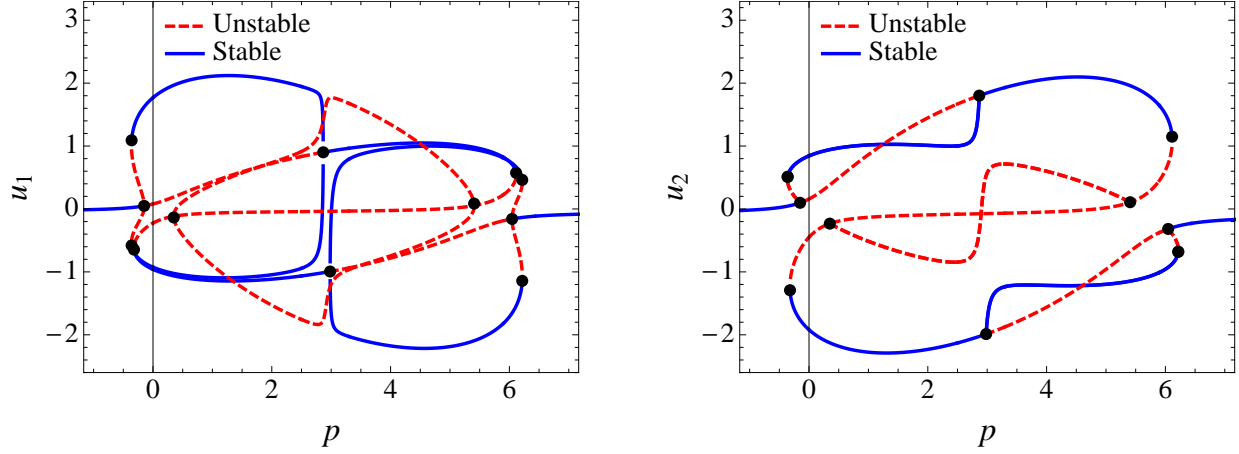


FIGURE 6. The global bifurcation diagram for the equilibrium solutions on $p-u_1$ and $p-u_2$ plane, in one of the symmetry breaking configurations. The perturbation is applied such that the spring force of the end spring is perturbed by making $a_3 = a + \varepsilon$ and $b_3 = b + \varepsilon$, for small epsilon. We have taken $\varepsilon = 0.1$, to show the symmetry breaking more clearly. The star bifurcation and the bifurcations at $p = y_1$, are unfolded revealing one of the configurations of the global perturbations. Here the solid blue curves represent the stable and the dotted red ones represent the unstable equilibrium solutions. The black dots are the bifurcation points in the perturbed system.

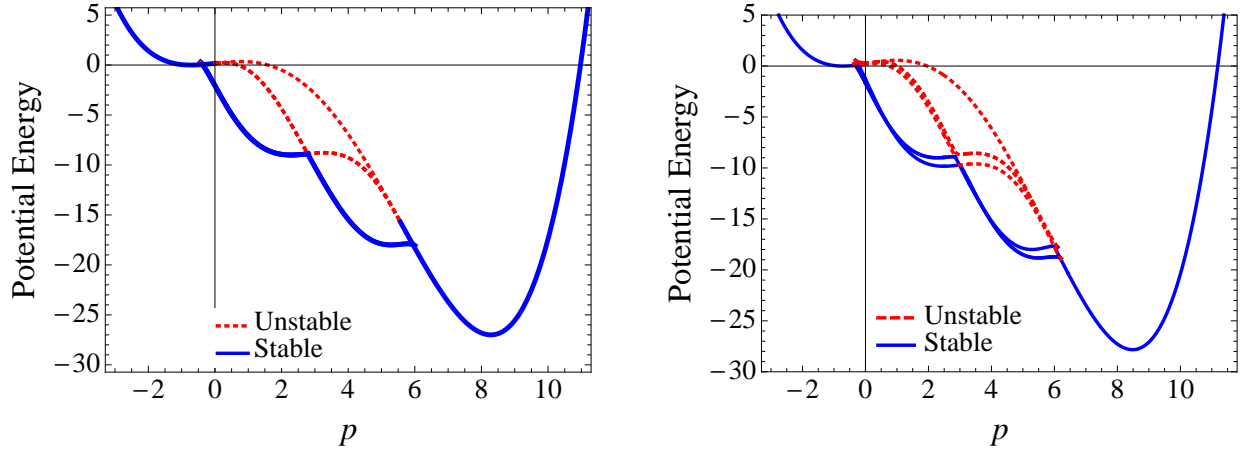


FIGURE 7. Total final potential energies of the 2DOF system. Left figure represents the symmetric case corresponding to the Figure 5 and the right figure correspond to the symmetry breaking in the Figure 6, that reveals the overlapping energy levels. This global symmetry breaking bifurcation diagram reveals the different levels of energies present in the global negative stiffness region of the system w.r.t. the pull parameter p . The energy levels in the solid blue curves correspond to stable and the dotted red ones correspond to the unstable equilibrium solutions.

3.2.1 Stability and Codimension of the Star Bifurcation.

In order to study the bifurcation behavior and degree of degeneracy of the star bifurcation, we find a normal form near B_1 . Local to the origin near $p = 0$, neglecting the cubic terms from equation (17), we get undamped EOM

$$\begin{aligned} \ddot{u}_1 &= h_1(u_1, u_2, p) = 2\gamma_1(2u_1 - u_2)\left(u_2 + \frac{2}{3}p\right) \\ \ddot{u}_2 &= h_2(u_1, u_2, p) = 2\gamma_1(u_1 - 2u_2)\left(u_1 - \frac{2}{3}p\right) \end{aligned} \quad (21)$$

Letting $p = \frac{3\hat{p}}{4\gamma_1}$, $u_1 = \frac{\hat{u}_1}{2\gamma_1}$, and $u_2 = \frac{\hat{u}_2}{2\gamma_1}$, the above equation is simplified to obtain a *normal form* as:

$$\begin{aligned} \ddot{\hat{u}}_1 &= \hat{h}_1(\hat{u}_1, \hat{u}_2, \hat{p}) = (2\hat{u}_1 - \hat{u}_2)(\hat{u}_2 + \hat{p}) \\ \ddot{\hat{u}}_2 &= \hat{h}_2(\hat{u}_1, \hat{u}_2, \hat{p}) = (\hat{u}_1 - 2\hat{u}_2)(\hat{u}_1 - \hat{p}) \end{aligned} \quad (22)$$

and the equilibrium solutions to the above normal form

$$(\hat{u}_1, \hat{u}_2) = \left\{ (0, 0), (\hat{p}, 2\hat{p}), (-2\hat{p}, -\hat{p}), (\hat{p}, -\hat{p}) \right\} \quad (23)$$

Now, for the stability analysis, the Jacobian of the second order form is computed from $\mathbf{J} = -\mathbf{D}\hat{\mathbf{h}}$, where $\hat{\mathbf{h}} = [\hat{h}_1, \hat{h}_2]^T$.

$$\mathbf{J} = \begin{pmatrix} -2(\hat{u}_2 + \hat{p}) & (2\hat{u}_2 - 2\hat{u}_1 + \hat{p}) \\ (2\hat{u}_2 - 2\hat{u}_1 + \hat{p}) & 2(\hat{u}_1 - \hat{p}) \end{pmatrix} \quad (24)$$

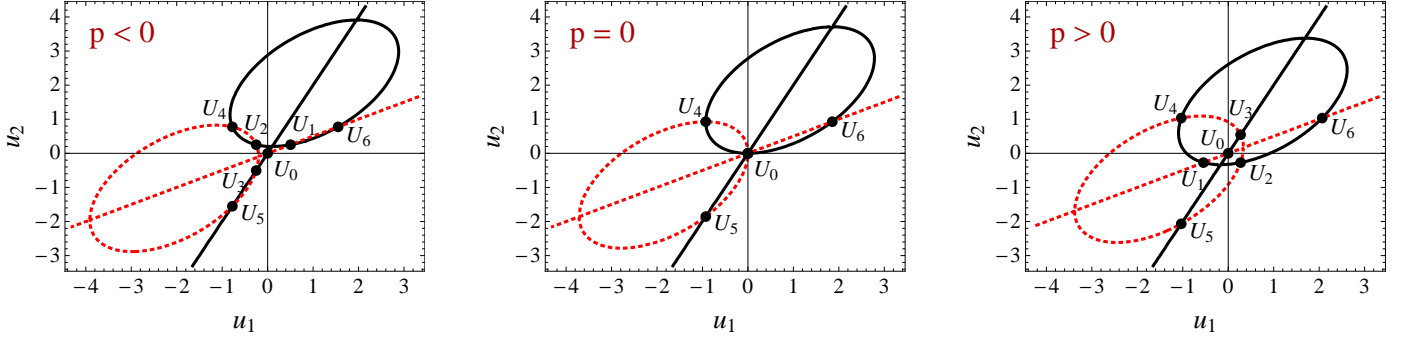


FIGURE 8. The equilibrium solutions projected onto the $u_1 - u_2$ plane and noted as $U = (u_1, u_2)$. The solid and dashed ellipses and straight lines satisfy $g_1(u_1, u_2, p) = 0$ and $g_2(u_1, u_2, p) = 0$ respectively. As p approaches zero from both directions the equilibrium solutions U_1, U_2 and U_3 converge into U_0 . For $p < 0$ the points U_1, U_2 and U_3 are unstable and become stable when $p > 0$. U_0 changes from stable to unstable as p goes from negative to positive. The stabilities of the points U_4, U_5 and U_6 remain stable on both sides local to $p = 0$.

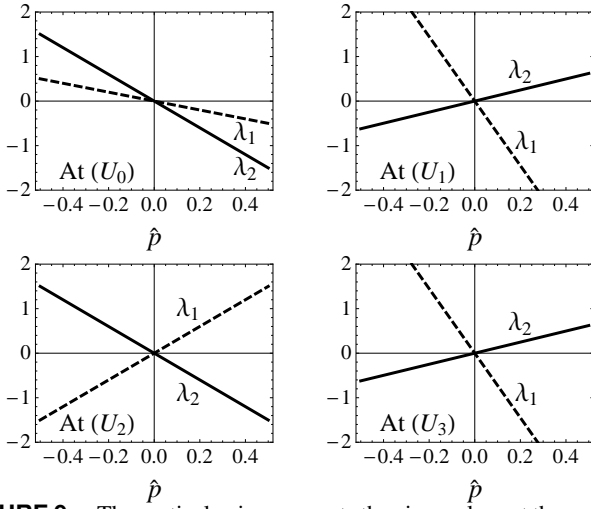


FIGURE 9. The vertical axis represents the eigenvalues at the equilibria in the normal form at the star bifurcation local to $\hat{p} = 0$. The points U_1, U_2 and U_3 remain unstable whereas the stability of U_0 changes from stable to unstable as \hat{p} goes from negative to positive.

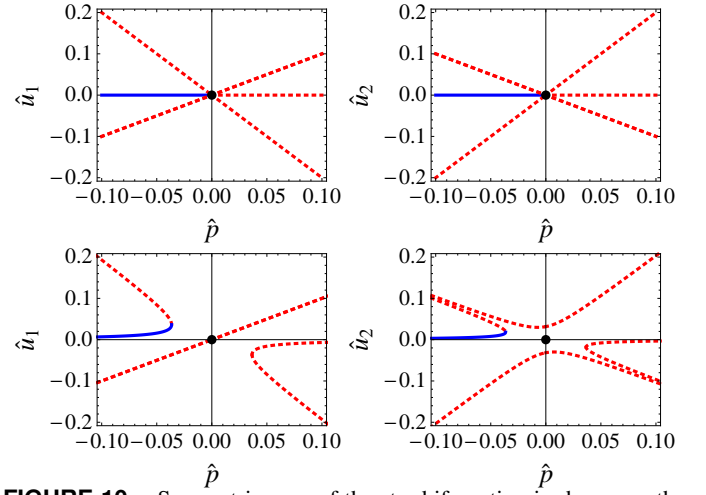


FIGURE 10. Symmetric case of the star bifurcation is shown on the top, and the bottom figures show the symmetry breaking of the star bifurcation, where $\{\hat{h}_1 + \varepsilon = 0, \hat{h}_2 = 0\}$. With reference to the symmetric case, overlapping projected branches are revealed.

The eigenvalues of the normal form are computed from the above Jacobian, at the equilibria obtained in the equation (23) and are illustrated in the Fig. 9. The behavior of these equilibria is illustrated in Figure 8. The dashed and solid ellipses and straight lines in Figure 8 satisfy $g_1(u_1, u_2, p) = 0$ and $g_2(u_1, u_2, p) = 0$ of equation (17) respectively. Points of intersection between a dashed and solid curve satisfy both equations, and hence are equilibrium points (u_1, u_2) , that are denoted by U_0, U_1, \dots, U_7 . The solutions of $\hat{h}_1(\hat{u}_1, \hat{u}_2, \hat{p}) = 0$ and $\hat{h}_2(\hat{u}_1, \hat{u}_2, \hat{p}) = 0$ correspond to the equilibria U_0, U_1, U_2 and U_3 in Figure 8. As \hat{p} passes through zero, these four equilibria are seen to collide at the origin, and then separate again. This is part of the star bifurcation. The stabilities are determined by the eigenvalues of the Jacobian, \mathbf{J} ; evaluated at the fixed points.

The eigenvalues of the second order system near the origin are as shown in Figure 9. Since it is a 2DOF system, we have obtained two eigenvalues in the second order form that results in four eigenvalues in the first order form. Therefore four eigenvalues going to zero as \hat{p} goes from negative to positive passing through $\hat{p} = 0$. The system with four eigenvalues simultaneously going to zero is referred to as a codimension four bifurcation [39, 40]. The bifurcation point B_2 is qualitatively similar to B_1 but from the opposite direction. Hence for the undamped symmetric 2DOF system there exist two codimension four "star bifurcations" B_1 and B_2 . However, for damped system, when we apply only one of the dampers i.e. making the damping coefficient from one of the dashpots to be zero, we get three zero eigenvalues and one negative purely real eigenvalue. From the definition of codimension this is a codimension three bifurcation. In presence

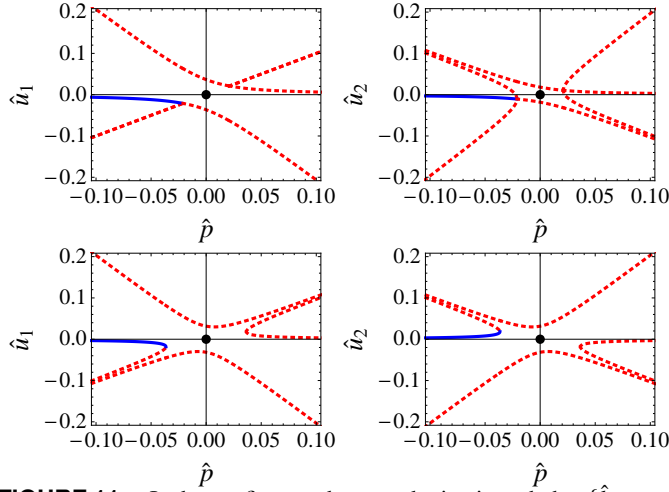


FIGURE 11. In the top figures, the perturbation is such that $\{\hat{h}_1 - \varepsilon = 0, \hat{h}_2 = 0\}$, where the branches with positive slope on $\hat{p} - \hat{u}_1$ plane are both two distinct, overlapping projected branches that is separated in the projection on the $\hat{p} - \hat{u}_2$ plane. In the bottom figures, $\{\hat{h}_1 - \varepsilon = 0, \hat{h}_2 + \varepsilon = 0\}$, where all the branches in $\hat{p} - \hat{u}_1$ and $\hat{p} - \hat{u}_2$ planes are revealed unfolding the star bifurcation into saddle nodes.

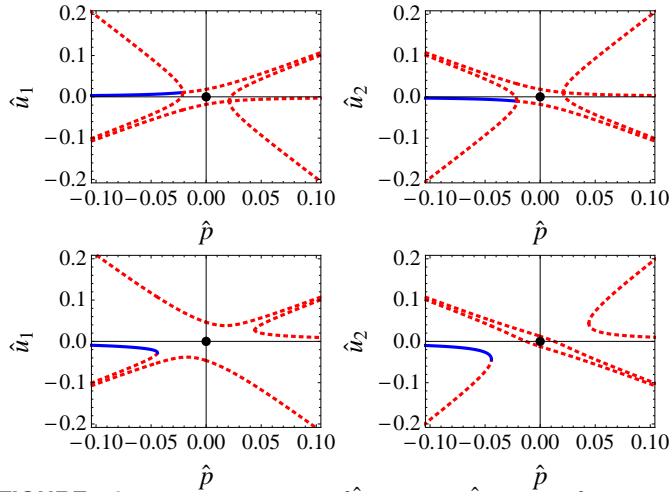


FIGURE 12. In the top figures $\{\hat{h}_1 + \varepsilon = 0, \hat{h}_2 - \varepsilon = 0\}$, the star bifurcation breaks into pitchfork bifurcations on both the \hat{u}_1 and \hat{u}_2 plane. Whereas in the bottom figures both the star bifurcations breaks into saddle-nodes, where $\{\hat{h}_1 - \varepsilon = 0, \hat{h}_2 - \varepsilon = 0\}$. Here the symmetry breaking on $\hat{p} - \hat{u}_1$ plane is qualitatively similar to the perturbation case $\{\hat{h}_1 - \varepsilon = 0, \hat{h}_2 + \varepsilon = 0\}$ shown in Figure 11. However this presents a different symmetry breaking configuration on $\hat{p} - \hat{u}_2$ plane

of both the dashpots two of the four eigenvalues are zero and the other two are negative and purely real, hence a codimension two bifurcation. Therefore depending on the nature of damping we get either codimension two or three star bifurcation at $\hat{p} = 0$.

At steady state equilibrium U_0 the four eigenvalues split from

real to imaginary going through zero as the parameter p passes through zero. At U_1 , U_2 and U_3 a set of two real and imaginary eigenvalues split into a set of imaginary and real eigenvalues respectively as the eigenvalues pass through $\hat{p} = 0$. For all of these four equilibrium curves, at $\hat{p} = 0$, the four eigenvalues for each equilibrium curve goes to zero, implying that each of these curves go through a codimension four bifurcation.

A global bifurcation behavior has been presented in Figure 6, for a particular symmetry breaking that reveals the overlapped branches in $\hat{p} - \hat{u}_1$ plane. Now to reveal the degeneracy at the star bifurcation point, we apply a small perturbation to the normal form, that results in the breaking and unfolding of the star bifurcation. The local normal form is studied for various types of perturbations on both $\hat{p} - \hat{u}_1$ and $\hat{p} - \hat{u}_2$ plane as shown in Figures 10, 11 and 12. We observed from the various perturbations that the star bifurcation changes to saddle-node and pitchfork bifurcations depending on the perturbation type, where the pitchforks can be further reduced to saddle-nodes with additional perturbation.

The global bifurcation diagram for the energy, provides insight into the optimum harvestable energy in the pull parameter region. Multiple energy levels exist in the negative stiffness region for the symmetry breaking case as seen in Figure 7. At a particular value of the pull parameter p in the negative stiffness region, depending on different initial conditions or different parameter values such as the mass and damping coefficients, the final energy lands on one of those levels. Therefore predicting the highest levels of harvestable energies in this region is difficult.

4 Conclusions and Outlook

In this paper we have presented a detailed bifurcation study of a twinkling oscillator. The spring mass twinkler consist of non-linear springs with cubic spring forces, and a quasistatic pull at the end spring. We show the SDOF and 2DOF system as examples of the twinklers. For SDOF we observed two local pitchfork bifurcations that are classified as codimension two bifurcations in undamped symmetric case. The symmetry breaking of the SDOF twinkler breaks the pitchfork into saddle-node. In 2DOF example however, we observe a complicated global bifurcation. A codimension four star bifurcation has been identified in the undamped 2DOF system that changes to codimension three or two for the damped system, depending on the nature of damping. We have shown different symmetry breaking cases for the star bifurcation that unfolds into saddle-node bifurcations.

This article gives insight into the dynamics of the SDOF and 2DOF twinkling oscillators, which is a building block for further analysis. The unstable branches of the star bifurcation will not be observable, but understanding them will help in understanding

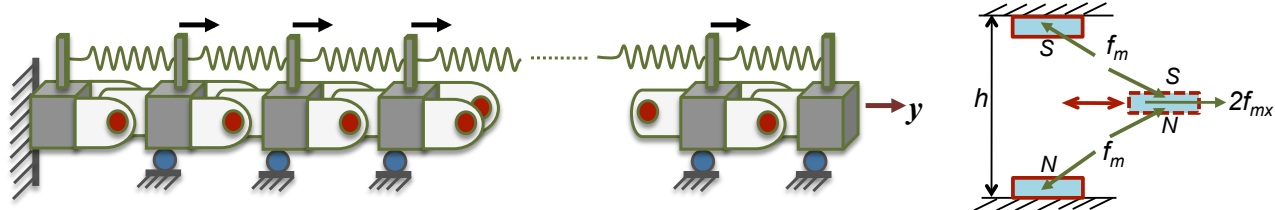


FIGURE 13. A possible arrangement of masses with magnets and linear spring to produce a chain of bistable systems. The masses consist of magnets shown in red which are arranged in a way that they repel each other. Each mass consist of 3 magnets, two on the right (sleeve) and one on the left (tongue) except for the first and the last mass. Here y is the quasistatic pull distance of the end spring. The right figure shows the repelling forces between the magnets on the tongue and the sleeves.

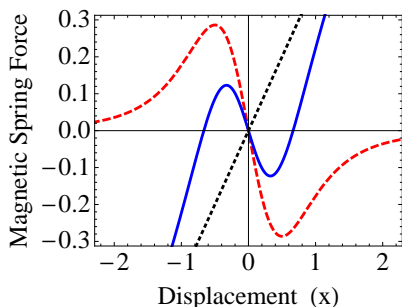


FIGURE 14. Total Magnetic spring force (solid blue curve) that can be achieved from combining the force due to magnets only (dashed red curve) and the linear spring force (dotted black line).

how transient vibrations settle to either of the equilibrium energy levels in symmetry breaking case.

Future work will include a more detailed study of the other bifurcations at points $B_7 - B_{10}$ (Figure 4), and a study of the existence of chaos through fractal basin boundaries and Lyapunov exponents. We also have plans for an experimental study. Mann and Sims [31] have developed a theoretical and experimental single-DOF model using permanent magnets to obtain a Duffing-like oscillator capable of harvesting energy by inducing current in the coils wrapped around the moving magnet. The same principle can be applied to harvest energy from the negative stiffness twinkling oscillator. We envision using permanent magnets arranged on the masses such that they create a negative stiffness or bistable system as shown in Figure 13, and connecting the masses through linear springs. Repulsive forces (f_m) between cylindrical permanent magnets [41] as between magnets on the the tongue and sleeve seen in the figure 13 have an x -component (f_{mx}) similar to the dashed red curve in Figure 14. Forces due to the magnets and the linear spring add up to form a nonlinear spring force shown as the solid blue curve in Figure 14. Alone, it has two stable equilibria and has a negative stiffness region. Later, energy harvesting in this system can be studied, for example, by converting the motion of the magnets into electric currents in coils wrapped around the magnets. (We may find more efficient ways to harvest the energy.) The system can be

preloaded to achieve the spring force qualitatively similar to Figure 2 and EOM as described in equation (1), including viscous damping and an equation for electrical damping.

ACKNOWLEDGMENT

This material is based upon work supported by the National Science Foundation under Grant No. CMMI-1030377. Any opinions, findings, and conclusions or recommendations expressed in this material are those of the authors and do not necessarily reflect the views of the National Science Foundation.

REFERENCES

- [1] Feeny, B. F., and Diaz, A. R., 2010. "Twinkling phenomena in snap-through oscillators". *Journal of Vibration and Acoustics*, **132**, p. 061013.
- [2] Wang, Y. C., and Lakes, R. S., 2004. "Extreme stiffness systems due to negative stiffness elements". *American Journal of Physics*, **72**, p. 40.
- [3] Puglisi, G., and Truskinovsky, L., 2000. "Mechanics of a discrete chain with bi-stable elements". *Journal of the Mechanics and Physics of Solids*, **48**(1), pp. 1–27.
- [4] Puglisi, G., and Truskinovsky, L., 2002. "Rate independent hysteresis in a bi-stable chain". *Journal of the Mechanics and Physics of Solids*, **50**(2), pp. 165–187.
- [5] Puglisi, G., 2006. "Hysteresis in multi-stable lattices with non-local interactions". *Journal of the Mechanics and Physics of Solids*, **54**(10), pp. 2060–2088.
- [6] Sarafian, H., 2010. "Static electric-spring and nonlinear oscillations". *Journal of Electromagnetic Analysis & Applications (JEMAA)*, **2**(2), pp. 75–81.
- [7] Sarafian, H., 2011. "Nonlinear oscillations of a magneto static spring-mass". *Journal of Electromagnetic Analysis and Applications*, **3**, pp. 133–139.
- [8] Roundy, S., and Wright, P. K., 2004. "A piezoelectric vibration based generator for wireless electronics". *Smart Materials and Structures*, **13**, p. 1131.

- [9] Sodano, H. A., Inman, D. J., and Park, G., 2005. "Comparison of piezoelectric energy harvesting devices for recharging batteries". *Journal of Intelligent Material Systems and Structures*, **16**(10), p. 799.
- [10] Liao, Y., and Sodano, H. A., 2008. "Model of a single mode energy harvester and properties for optimal power generation". *Smart Materials and Structures*, **17**, p. 065026.
- [11] Renno, J. M., Daqaq, M. F., and Inman, D. J., 2009. "On the optimal energy harvesting from a vibration source". *Journal of Sound and Vibration*, **320**(1-2), pp. 386–405.
- [12] Scruggs, J. T., and Behrens, S., 2011. "Optimal energy harvesting from low-frequency bistate force loadings". *Journal of Vibration and Acoustics*, **133**, p. 011008.
- [13] Anton, S. R., and Sodano, H. A., 2007. "A review of power harvesting using piezoelectric materials (2003–2006)". *Smart Materials and Structures*, **16**, p. R1.
- [14] Stanton, S. C., Erturk, A., Mann, B. P., and Inman, D. J., 2010. "Nonlinear piezoelectricity in electroelastic energy harvesters: Modeling and experimental identification". *Journal of Applied Physics*, **108**(7), pp. 074903–074903.
- [15] Stanton, S. C., McGehee, C. C., and Mann, B. P., 2010. "Nonlinear dynamics for broadband energy harvesting: Investigation of a bistable piezoelectric inertial generator". *Physica D: Nonlinear Phenomena*, **239**(10), pp. 640–653.
- [16] Kim, S., Clark, W. W., and Wang, Q. M., 2005. "Piezoelectric energy harvesting with a clamped circular plate: experimental study". *Journal of Intelligent Material Systems and Structures*, **16**(10), p. 855.
- [17] Mo, C., Radziemski, L. J., and Clark, W. W., 2010. "Experimental validation of energy harvesting performance for pressure-loaded piezoelectric circular diaphragms". *Smart Materials and Structures*, **19**, p. 075010.
- [18] Kerschen, G., McFarland, D. M., Kowtko, J. J., Lee, Y. S., Bergman, L. A., and Vakakis, A. F., 2007. "Experimental demonstration of transient resonance capture in a system of two coupled oscillators with essential stiffness nonlinearity". *Journal of Sound and Vibration*, **299**(4-5), pp. 822–838.
- [19] Quinn, D. D., Triplett, A. L., Bergman, L. A., and Vakakis, A. F., 2011. "Comparing linear and essentially nonlinear vibration-based energy harvesting". *Journal of Vibration and Acoustics*, **133**, p. 011001.
- [20] Quinn, D. D., Triplett, A. L., Vakakis, A. F., and Bergman, L. A., 2011. "Energy harvesting from impulsive loads using intentional essential nonlinearities". *Journal of Vibration and Acoustics*, **133**, p. 011004.
- [21] McFarland, D. M., Bergman, L. A., and Vakakis, A. F., 2005. "Experimental study of non-linear energy pumping occurring at a single fast frequency". *International Journal of Non-Linear Mechanics*, **40**(6), pp. 891–899.
- [22] Gourdon, E., Alexander, N. A., Taylor, C. A., Lamarque, C. H., and Pernot, S., 2007. "Nonlinear energy pumping under transient forcing with strongly nonlinear coupling: Theoretical and experimental results". *Journal of Sound and Vibration*, **300**(3-5), pp. 522–551.
- [23] Manevitch, L. I., Musienko, A. I., and Lamarque, C. H., 2007. "New analytical approach to energy pumping problem in strongly nonhomogeneous 2dof systems". *Meccanica*, **42**(1), pp. 77–83.
- [24] Tsakirtzis, S., Panagopoulos, P. N., Kerschen, G., Gendelman, O., Vakakis, A. F., and Bergman, L. A., 2007. "Complex dynamics and targeted energy transfer in linear oscillators coupled to multi-degree-of-freedom essentially nonlinear attachments". *Nonlinear Dynamics*, **48**(3), pp. 285–318.
- [25] Quinn, D. D., Gendelman, O., Kerschen, G., Sapsis, T. P., Bergman, L. A., and Vakakis, A. F., 2008. "Efficiency of targeted energy transfers in coupled nonlinear oscillators associated with 1:1 resonance captures: Part i". *Journal of Sound and Vibration*, **311**(3-5), pp. 1228–1248.
- [26] Sapsis, T. P., Vakakis, A. F., Gendelman, O. V., Bergman, L. A., Kerschen, G., and Quinn, D. D., 2009. "Efficiency of targeted energy transfers in coupled nonlinear oscillators associated with 1:1 resonance captures: Part ii, analytical study". *Journal of Sound and Vibration*, **325**(1-2), pp. 297–320.
- [27] Vakakis, A., Gendelman, O., Bergman, L., McFarland, D., Kerschen, G., and Lee, Y. S., 2009. *Nonlinear Targeted Energy Transfer in Mechanical and Structural Systems: I and II*. Springer.
- [28] Bellet, R., Cochelin, B., Herzog, P., and Mattei, P. O., 2010. "Experimental study of targeted energy transfer from an acoustic system to a nonlinear membrane absorber". *Journal of Sound and Vibration*, **329**(14), pp. 2768–2791.
- [29] Priya, S., and Inman, D. J., 2008. *Energy harvesting technologies*. Springer.
- [30] Stephen, N. G., 2006. "On energy harvesting from ambient vibration". *Journal of Sound and Vibration*, **293**(1-2), pp. 409–425.

- [31] Mann, B. P., and Sims, N. D., 2009. “Energy harvesting from the nonlinear oscillations of magnetic levitation”. *Journal of Sound and Vibration*, **319**(1-2), pp. 515–530.
- [32] Kurs, A., Karalis, A., Moffatt, R., Joannopoulos, J. D., Fisher, P., and Soljačić, M., 2007. “Wireless power transfer via strongly coupled magnetic resonances”. *Science*, **317**(5834), p. 83.
- [33] Karalis, A., Joannopoulos, J. D., and Soljacic, M., 2008. “Efficient wireless non-radiative mid-range energy transfer”. *Annals of Physics*, **323**(1), pp. 34–48.
- [34] Wei, X. C., Li, E. P., Guan, Y. L., and Chong, Y. H., 2009. “Simulation and experimental comparison of different coupling mechanisms for the wireless electricity transfer”. *Journal of Electromagnetic Waves and Applications*, **23**(7), pp. 925–934.
- [35] Kurs, A., Moffatt, R., and Soljacic, M., 2010. “Simultaneous mid-range power transfer to multiple devices”. *Applied Physics Letters*, **96**(4), pp. 044102–044102.
- [36] Peng, L., Breinbjerg, O., and Mortensen, N. A., 2010. “Wireless energy transfer through non-resonant magnetic coupling”. *Journal of Electromagnetic Waves and Applications*, **24**, **11**(12), pp. 1587–1598.
- [37] Peng, L., Wang, J. Y., Ran, L. X., Breinbjerg, O., and Mortensen, N. A., 2011. “Performance analysis and experimental verification of mid-range wireless energy transfer through non-resonant magnetic coupling”. *Journal of Electromagnetic Waves and Applications*, **25**, **5**(6), pp. 845–855.
- [38] Tesla, N., 1914. Apparatus for transmitting electrical energy. US Patent 1,119,732.
- [39] Nayfeh, A. H., and Balachandran, B., 1995. *Applied nonlinear dynamics: analytical, computational, and experimental methods*. Wiley.
- [40] Wiggins, S., 2003. *Introduction to applied nonlinear dynamical systems and chaos*, Vol. 2. Springer.
- [41] Agashe, J. S., and Arnold, D. P., 2008. “A study of scaling and geometry effects on the forces between cuboidal and cylindrical magnets using analytical force solutions”. *Journal of Physics D: Applied Physics*, **41**, p. 105001.